2024 46th Annual International Conference of the IEEE Engineering in Medicine and Biology Society (EMBC) | 979-8-3503-7149-9/24/$31.00 ©2024 IEEE | DOI: 10.1109/EMBC53108.2024.10782873

Revealing Alzheimer's Disease Dementia Patterns in [18F]Florbetapir PET with Independent Component Analysis

Nigar Khasayeva
Tri-Institutional Center for Translational Research in Neuroimaging and Data Science (TReNDS), Georgia State University, Atlanta, GA, USA
nkhasayeva1@gsu.edu

Cyrus Eierud
Tri-Institutional Center for Translational Research in Neuroimaging and Data Science (TReNDS), Georgia State University, Atlanta, GA, USA
ceierud@gsu.edu

Kyle M. Jensen
Tri-Institutional Center for Translational Research in Neuroimaging and Data Science (TReNDS), Georgia State University, Atlanta, GA, USA
kjensen7@gsu.edu

Enrico Premi
Stroke Unit, ASST Spedali Civili, Spedali Civili Hospital, Brescia, Italy
zedtower@gmail.com

Barbara Borroni
Department of Clinical and Experimental Sciences, University of Brescia, Italy; Department of Continuity of Care and Frailty, ASST Spedali Civili Brescia, Italy
barbara.borroni@unibs.it

Vince D. Calhoun
Tri-Institutional Center for Translational Research in Neuroimaging and Data Science (TReNDS), Georgia State University, Atlanta, GA, USA
vcalhoun@gsu.edu

Armin Iraji
Tri-Institutional Center for Translational Research in Neuroimaging and Data Science (TReNDS), Georgia State University, Atlanta, GA, USA
airaji@gsu.edu

***Abstract*— This study investigates Alzheimer's Disease (AD) dementia through [18F]Florbetapir ([18F]FBP) Positron Emission Tomography (PET) imaging. We employ Independent Component Analysis (ICA) to identify shared latent patterns across controls and individuals with Dementia. The dataset comprises PET brain images from 440 participants from the Alzheimer's Disease Neuroimaging Initiative (ADNI). After visual inspection, nine independent components (IC) were selected, including visual, salience, default mode, cerebellum, left and right temporal, motor, frontal, and subcortical/brainstem. A Generalized Linear Model (GLM) analysis was performed on the IC weights to evaluate group differences. Salience, default mode, left and right temporal, and frontal components displayed a significant group effect with increased weights in the AD dementia group. Notably, the salience and frontal components demonstrated a significant interaction effect of diagnosis with age. This study emphasizes the potential of ICA in conjunction with [18F]FBP PET imaging to provide valuable insights into the neurobiology of AD dementia.**

Keywords*— *Positron Emission Tomography, Florbetapir, Dementia, Alzheimer's disease, Independent Component Analysis

I. INTRODUCTION

Dementia is an age-related neurological condition that induces a gradual decline in cognitive abilities, including memory, language, problem-solving skills, and overall executive function. Alzheimer's Disease (AD) is a prominent form of dementia that has been characterized as a pathology primarily affecting gray matter, marked by the deposition of amyloid-β (Aβ) plaques and neurofibrillary tangles [1]. Positron Emission Tomography (PET) is a non-invasive imaging technique that can provide valuable insights into neurodegenerative brain disorders, including various types of dementia. PET imaging depends on the use of specialized radioactive tracers injected into the body. In our study, we employed [18F]Florbetapir ([18F]FBP), an Aβ targeting radiotracer. This tracer has demonstrated high accuracy in detecting Aβ plaques [2], a crucial element in AD diagnosis. [18F]FBP has also shown its potential in recent PET studies for identifying uptake variations within the brain, particularly those associated with AD dementia.

A common approach to studying PET data involves using predefined region of interest (ROI) based analysis to detect these variations. The ROI approach involves analyzing average tracer uptake within predefined brain regions. However, it relies heavily on a few predefined anatomical locations and falls short of covering the entire brain space [3]. Moreover, different voxels within the same ROI may not exhibit the same tracer uptake pattern due to subject differences or variations in disease impact. Voxel-based analysis [4], on the other hand, evaluates each voxel independently. It provides a more granular view of tracer distribution, potentially capturing variations that might be averaged out in an ROI-based analysis. Additionally, it does not require predefined ROIs and can cover the whole brain space. Nevertheless, this approach is univariate, analyzing each voxel independently, it can overlook potential relationships among them. This is a limitation that ROI analysis shares as well. Furthermore, meaningful patterns may not survive multiple comparison corrections due to the substantial number of statistical tests involved. Multivariate data-driven methods present a promising solution to address mentioned above challenges by extracting information across voxels. One such method is Independent Component Analysis (ICA), which is used to extract latent sources defined as groups of voxels carrying similar information. These sources manifest covariance across subjects and highlight discernible differences between groups [5].

ICA has been increasingly utilized in the analysis of PET data. In a previous study [6], ICA was performed on [18F]Fluorodeoxyglucose ([18F]FDG; another type of radiotracer) PET data to reveal insight into the spatial distribution of aging effects on the brain. They performed ICA with a relatively high number of Independent Components (IC), finding several regions with reductions in local metabolic activity during aging, including the bilateral anterior temporal lobe and orbitofrontal cortex. These identified regions demonstrated causal effects to other regions such as subcortical regions, inferior frontal cortex, left temporal cortex, and posterior visual regions, thereby supporting the interregional extent of age effects in the brain. Another study employed Parallel ICA on both [18F]FDG PET and [11C]Pittsburgh Compound-B ([11C]PiB) PET data from a population of individuals with probable AD [7]. They found three components in [18F]FDG PET associated with language and visuospatial functions. The components related to visuospatial function closely resembled a high-order visual network and a right hemisphere posterior default mode network. To our knowledge, the application of ICA data-driven methods on [18F]FBP PET data remains unexplored. Despite existing PET research with other tracers, applying ICA to [18F]FBP PET unveils latent factors, contributing to a more comprehensive understanding of the neurobiology of AD dementia and complements existing studies using different tracers.

The objective of the current study is to leverage data-driven approach to detect significant changes in uptake between controls and individuals with dementia. To achieve this, we applied ICA to [18F]FBP PET data and examined the influence of diagnostic conditions on [18F]FBP-related components.

II. Materials and Methods

A. Participants

The initial dataset comprised PET brain images from 897 participants from the Alzheimer's Disease Neuroimaging Initiative (ADNI). A subset of data comprising resting-state fMRI scans collected within a ±180 days tolerance from the scan date originally gathered for another ongoing investigation, has been utilized in this study. Subjects missing diagnostic information were excluded from the analysis, and the rest were classified into two groups based on their diagnostic information: Controls and Individuals with Dementia. Individuals with Mild Cognitive Impairment (MCI) were excluded. The resulting dataset used in our analysis comprised 440 subjects (controls = 292, individuals with dementia = 148).

TABLE I. Demographics of the Study Group

Diagnostic	N	Sex	N	Age (mean ± SD)
Control Group	292	Male	122	72.94 ± 6.70
		Female	170	70.75 ± 6.44
Dementia Group	148	Male	79	74.98 ± 7.58
		Female	69	71.70 ± 7.76

SD, Standard Deviation

B. Image Acquisition and Preprocessing

All images were collected after participants were injected with the [18F]FBP tracer to measure amyloid deposition. Prior to analysis, the acquired images underwent preprocessing steps, including spatial normalization to a standard anatomical template using SPM (http://www.fil.ion.ucl.ac.uk/spm/). The standardized uptake ratio (SUVR) was calculated using the cerebellar gray matter as a reference region to normalize the tracer uptake value. The cerebellar gray matter is commonly used as a reference region due to [18F]FBP PET targeting prevalently Aβ plaques that are notably less evident in the cerebellum [8]. Additionally, smoothing with a 10mm Gaussian kernel and resampling to 3×3×3 mm resolution with AFNI (https://afni.nimh.nih.gov) were performed.

C. Independent Component Analysis (ICA)

ICA is a blind-source separation method [9] used for extracting and separating statistically ICs from input data which is assumed to include mixed signals, both signals of interest and signals not of interest (noise). The interplay between the observed PET data matrix (X), independent source matrix (S), and the loading matrix (A) is mathematically captured by (1):

$$X = A \times S \tag{1}$$

Within our study, we performed ICA with a model order of 20 after concatenating data from all subjects. We used the Infomax algorithm and leveraged ICASSO module of Group ICA of fMRI Toolbox [10] (GIFT v4.0c, https://github.com/trendscenter/gift) to obtain reliable ICs. Nine components were selected and manually labeled by experts in our research group after the exclusion of ventricle, white matter, and artifact components. We used the loading matrix (A), which represents the weights selected sources contributing to each of the 440 subjects for further analysis.

D. Generalized Linear Model (GLM)

We performed a Generalized Linear Model (GLM) to analyze the weights extracted from each of the nine ICs. This analysis aimed to assess differences across groups. Each IC's weight was modeled as a linear combination of several covariates, including age, gender, site, and diagnostic status. We developed an interaction model, represented as IC Weight ~ Diagnosis + Age + Gender + Site + (Age × Diagnosis), to investigate how the diagnosis covariate and its interaction with age influenced the variation in component weight.

Our primary objective was to identify significant effects associated with diagnosis and its age interaction effects for each IC, using a significance threshold of $\alpha = 0.05$. To account for multiple comparisons, we applied a False Discovery Rate (FDR) correction using the Benjamini-Hochberg method [11].

III. Results

Using a model order of 20, we identified nine ICs after excluding ventricle, white matter, and artifactual components: visual, salience, default mode, cerebellum, left temporal, right temporal, motor, frontal, and subcortical/brainstem (Fig. 1). We then assessed the impact of diagnosis and its interaction with age on these components. We found significant diagnostic effects in default mode ($p < 0.005$), right temporal ($p < 0.05$), and left temporal ($p < 0.005$) (Fig. 2). Additionally, two of these components, the salience and frontal components, displayed significant interaction effects ($p < 0.05$) (Fig. 3). All five of these components exhibited increased weights in the dementia group compared to the control group.

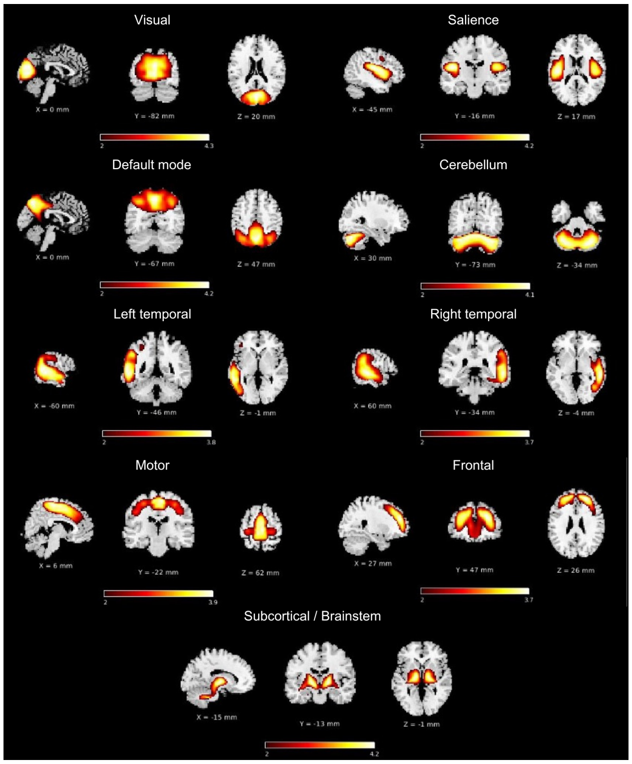

Fig. 1. Spatial maps for nine components extracted through Independent Component Analysis

IV. Discussion

Our study leverages ICA and [18F]FBP PET imaging to identify nine distinct components in the brain: visual, salience, default mode, cerebellum, left and right temporal, motor, frontal, and subcortical/brainstem.

Among these components, five exhibited significant differences in component weights between individuals with AD dementia and controls, with increased weights observed in the AD dementia group. This elevation in component weights suggests higher [18F]FBP signal intensity, indicative of elevated Aβ plaque deposition in the brain. These findings align with existing literature that establishes a relationship between an increase in Aβ plaques and the progression of AD [12]. The identified components, particularly those exhibiting significant differences in component weights between AD dementia and control groups, encompass brain regions implicated in the pathophysiology of dementia. For instance, alterations in the default mode component, which is involved in introspective and self-referential processes, have been consistently reported in AD. It has been suggested that more Aβ plaques accumulate within the brain areas that compose the default mode networks (DMN) as a result of the high metabolic rate of its continuous activation [13]. These plaques may disrupt the neural mechanisms of brain structures within the DMN, such as the precuneus, posterior cingulate cortex, and angular gyrus. These structures are associated with cognitive processes such as memory formation and retrieval and a disruption in these processes may account for the symptoms of AD [14]. The involvement of both temporal and default mode components in AD dementia aligns with the structural and functional impairments observed through various imaging techniques such as fMRI and [18F]FDG PET [15]. Increased component weights in regions associated with the salience and frontal components, which are involved in cognitive control and attention, further emphasize the cognitive deficits characteristic of AD [16]. Additionally, an interaction effect with age was observed for the salience and frontal components. Specifically, as age increased, there was a relative reduction in amyloid deposition. Even if this can be partially explained considering individual differences of AD dementia group [17], this finding also supports the complex relationship between amyloid deposition and its local and distant effects. Interestingly, these two components are less involved in the initial phase of the disease [18], suggesting they might serve a compensatory role.

While PET provides valuable insights, it is not the only imaging modality that can shed light on the complexities of AD dementia [19]. Our findings align with previous fMRI studies that have reported the influence of AD on these components [20]. Combining PET and fMRI in a multimodal approach can provide a more comprehensive study of the AD dementia effects on the brain, providing both anatomic and functional information. This is where the integration of multimodal fusion proves pivotal. As we progress, our research will focus on the application of multimodal ICA to both fMRI and PET data. This approach will enable us to conduct an exhaustive examination of the changes associated with AD dementia, thereby improving our ability to monitor this disease.

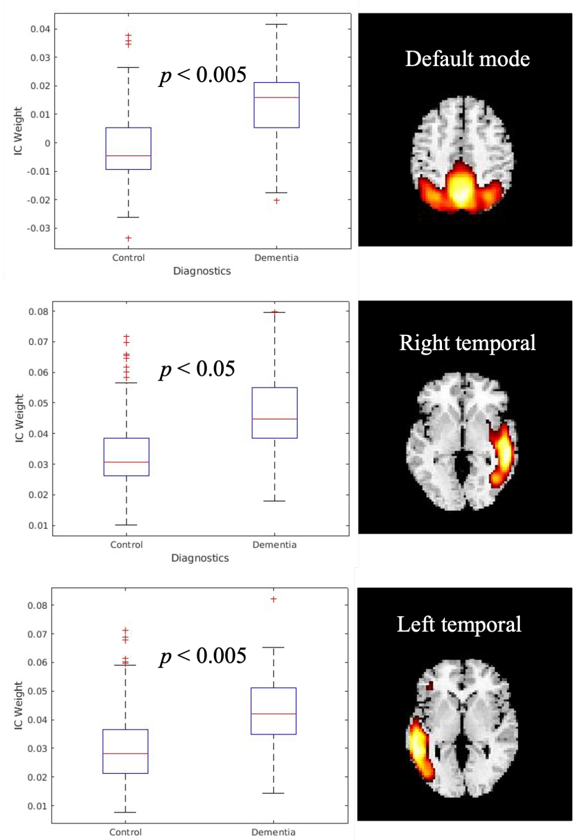

Fig. 2. Significant Group Effects in uptake differences in Individuals with Dementia: Relationship between Independent Component (IC) weight and diagnostic groups.

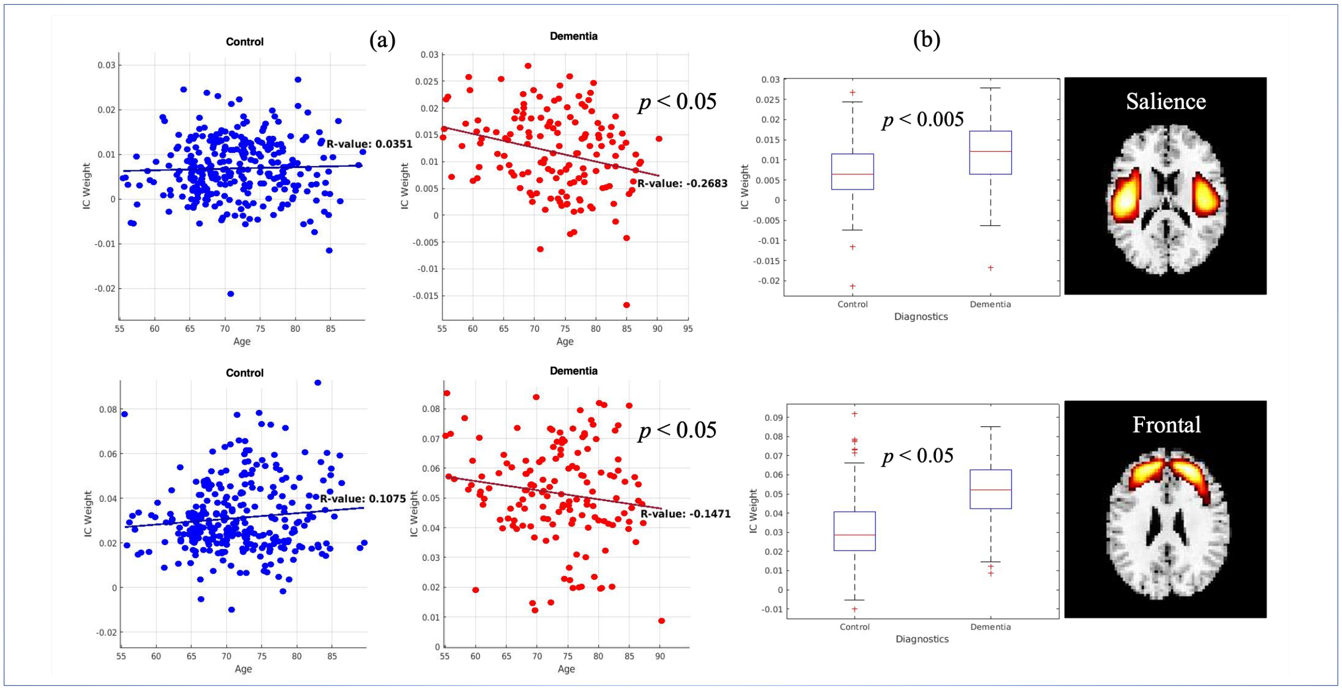

Fig. 3. Significant Age-Diagnosis Interaction Effects in uptake differences in Individuals with Dementia: (a) Fitted Regression Lines illustrating the Relationship between Age and Independent Component (IC) weight, (b) Relationship between IC weight and diagnostic groups.

V. Conclusion

ICA approach was applied on anatomical information from [18F]FBP PET imaging to extract a component-based distribution of amyloid deposition across the whole brain. We identified nine brain components, five of which exhibited significant differences between the dementia and control groups. We then provided insights utilizing these identified components, elucidating the pathophysiology of AD dementia, and highlighting potential targets for further investigation and intervention.

References

[1] C. R. Jack and D. M. Holtzman, "Biomarker Modeling of Alzheimer's Disease," Neuron, vol. 80, no. 6, pp. 1347–1358, Dec. 2013, doi: 10.1016/j.neuron.2013.12.003.

[2] Clark, C.M. et al., Use of florbetapir-PET for imaging beta-amyloid pathology. JAMA 2011, 305, 275–283.

[3] S. Aalto et al., "Reproducibility of automated simplified voxel-based analysis of PET amyloid ligand [11C]PIB uptake using 30-min scanning data" Eur J Nucl Med Mol Imaging, vol. 36, no. 10, pp. 1651–1660, Oct. 2009, doi: 10.1007/s00259-009-1174-1.

[4] J. Shin et al., "Voxel-based analysis of Alzheimer's disease PET imaging using a triplet of radiotracers: PIB, FDDNP, and FDG," NeuroImage, vol. 52, no. 2, pp. 488–496, Aug. 2010, doi: 10.1016/j.neuroimage.2010.04.013.

[5] L. Xu, K. M. Groth, G. Pearlson, D. J. Schretlen, and V. D. Calhoun, "Source‐based morphometry: The use of independent component analysis to identify gray matter differences with application to schizophrenia," Human Brain Mapping, vol. 30, no. 3, pp. 711–724, 2009, doi: 10.1002/hbm.20540.

[6] X. Di et al., "Interregional causal influences of brain metabolic activity reveal the spread of aging effects during normal aging," Human Brain Mapping, vol. 40, no. 16, pp. 4657–4668, Nov. 2019, doi: 10.1002/hbm.24728.

[7] R. Laforce et al., "Parallel ICA of FDG-PET and PiB-PET in three conditions with underlying Alzheimer's pathology," NeuroImage: Clinical, vol. 4, pp. 508–516, 2014, doi: 10.1016/j.nicl.2014.03.005.

[8] C. C. Rowe and V. L. Villemagne, "Brain Amyloid Imaging," J Nucl Med, vol. 52, no. 11, pp. 1733–1740, Nov. 2011, doi: 10.2967/jnumed.110.076315.

[9] N. Correa, T. Adalı, and V. D. Calhoun, "Performance of blind source separation algorithms for fMRI analysis using a group ICA method," Magnetic Resonance Imaging, vol. 25, no. 5, pp. 684–694, 2007, doi: 10.1016/j.mri.2006.10.017.

[10] A. Iraji, A. Faghiri, N. Lewis, Z. Fu, S. Rachakonda, and V. D. Calhoun, "Tools of the trade: estimating time-varying connectivity patterns from fMRI data," Social Cognitive and Affective Neuroscience, vol. 16, no. 8, pp. 849–874, Aug. 2021, doi: 10.1093/scan/nsaa114.

[11] Y. Benjamini and Y. Hochberg, "Controlling the False Discovery Rate: A Practical and Powerful Approach to Multiple Testing," Journal of the Royal Statistical Society Series B, vol. 57, no. 1, pp. 289–300, Jan. 1995, doi: 10.1111/j.2517-6161.1995.tb02031.x.

[12] W. Tsering and S. Prokop, "Neuritic Plaques — Gateways to Understanding Alzheimer's Disease," Mol Neurobiol, Nov. 2023, doi: 10.1007/s12035-023-03736-7.

[13] R. L. Buckner, J. R. Andrews‐Hanna, and D. L. Schacter, "The Brain's Default Network: Anatomy, Function, and Relevance to Disease," Annals of the New York Academy of Sciences, vol. 1124, no. 1, pp. 1–38, Mar. 2008, doi: 10.1196/annals.1440.011.

[14] H. Jahn, "Memory loss in Alzheimer's disease," Dialogues in Clinical Neuroscience, vol. 15, no. 4, pp. 445–454, 2013, doi: 10.31887/DCNS.2013.15.4/hjahn.

[15] J. Kim, M. Jeong, W. R. Stiles, and H. S. Choi, "Neuroimaging Modalities in Alzheimer's Disease: Diagnosis and Clinical Features," IJMS, vol. 23, no. 11, p. 6079, May 2022, doi: 10.3390/ijms23116079.

[16] W. Seeley, "The Salience Network: A Neural System for Perceiving and Responding to Homeostatic Demands," J. Neurosci., vol. 39, no. 50, pp. 9878–9882, Dec. 2019, doi: 10.1523/JNEUROSCI.1138-17.2019.

[17] F. Pan et al., "Sex and APOE genotype differences in amyloid deposition and cognitive performance along the Alzheimer's Continuum," Neurobiology of Aging, vol. 130, pp. 84–92, Oct. 2023, doi: 10.1016/j.neurobiolaging.2023.06.013.

[18] J. Zhou et al., "Divergent network connectivity changes in behavioural variant frontotemporal dementia and Alzheimer's disease," Brain, vol. 133, no. 5, pp. 1352–1367, 2010, doi: 10.1093/brain/awq075.

[19] P. N. E. Young et al., "Imaging biomarkers in neurodegeneration: current and future practices," Alz Res Therapy, vol. 12, no. 1, p. 49, Dec. 2020, doi: 10.1186/s13195-020-00612-7.

[20] F. Agosta et al., "Resting state fMRI in Alzheimer's disease: beyond the default mode network," Neurobiology of Aging, vol. 33, no. 8, pp. 1564–1578, Aug. 2012, doi: 10.1016/j.neurobiolaging.2011.06.007